ISSN: 2278-4632
Vol-13, Issue-12, December 2023

An Efficient Inductive Power Transfer Topology for Electric Vehicle Battery Charging

Gutti Siva Abhinash Research scholar, dept. of electrical and electronics engineering, Chirala Engineering College, Chirala.

P.S.K.L. Anuhya Assistant Professor, dept. of electrical and electronics engineering, Chirala Engineering College, Chirala.

ABSTRACT

Recently available high-frequency power converter topologies for inductive power transfer (IPT) system utilize either zero voltage switching (ZVS) or zero current switching (ZCS) based power electronic converters while maintaining a near sinusoidal current for limited power transfer range. However, achieving ZVS or ZCS for all power switches simultaneously is still a challenging task in IPT systems. In this article, an improved zero-voltage zero-current switching (ZVZCS) IPT topology and its switching pattern are proposed. ZVS is achieved by optimizing the classical series compensation and additionally, an auxiliary network is employed to achieve ZCS. The proposed concept is verified by using MATLAB/Simulink based simulations for resistive and battery load. An efficiency of 91.26% is achieved with ZVZCS for a full dynamic power transfer range of 20 W–1.1 kW.

Keywords: **PWM, Soft switching, Battery and Inductive power transfer.**

I. INTRODUCTION

Global frugality is declining, while energy reserves are being destroyed and the environment is being dangerously degraded. Additionally, it has aided in the development of green technologies that result in discoveries in the nations that produce the most CO2, or the top emitters of CO2. H. Transport, 1 and 2. Therefore, electric vehicles (EVs) have been advocated to reduce the environmental impact of carbon-based energy [2], [3]. Similarly, the demand for electric vehicles presents new opportunities for mortals to extend the life of their vehicles at lower costs [1],[3]. Historically, battery technology (BT) and power shaping technology have been limitations that have prevented the success of electric vehicles. Nevertheless, BT has been further developed over the decades with high energy viscosity, low weight and high potency [4].

Also, effective energy storage devices in conjunction with appropriate power shaping circuitry will improve overall performance. DC-DC exercise configurations with negligible power loss, continuity, the experimenter and their focus conduct consistent energy transfer and increase the number of charge-discharge cycles [1] through [4]. An effective short-range high-speed court is now stationed at the Lethal Security Company. In the current script, the grounding typology is represented using inductive power transfer (IPT) as a result of safer battery charging (BC) in both the fixed and moving modes of electric cars. To lower the circuit impedance and enhance the motor's overall efficiency, a compensation network is offered.

However, the complexity of the arrangement is correlated with the number of active and unstable foundations in the circuit [5]. The proper outcomes enhance end-user economics, maintenance cycles, decreased carbon footprint, and cruising range. As a result, the choice of motor is crucial in the increasing number of EVs. Therefore, it fully supports mitigation of environmental problems caused by traffic problems [6]). The conventional grounded IPT topology has One of Diligence's most popular network topologies is series-series capacitor compensation because of its simple construction and operational dependability across various coil spacing's [7]. The effectiveness, power handling capacity, high reverberation peaks, and control granularity of this network are compromised despite the fact that it produces inexpensive outcomes under varying loads. Presents a phase control algorithm to increase the efficiency bandwidth. Nevertheless, the output leads to advanced control strategies of variable frequency. In [8], defining control limits at the optimal frequency range mitigates problems caused by variable frequency. Control results in [7] and [8] only support bones.

To boost efficiency, keep zero voltage switching (ZVS) active in IPT systems. The topology of [9] was improved by the use of a unique coil support network with an intermediately adjusted on both the transmitting and reception sides; there is an L-C series structure. Even though the amount of weight on the vehicle side is increased with this layout, placing both coils on his main side [10] saves weight. In misaligned situations, the findings provided in [9] and [10] offer great flow support,

ISSN: 2278-4632
Vol-13, Issue-12, December 2023

but they limit the ease of the computational and control operations.

II OPERATING PRINCIPLE OF THE PROPOSED CONVERTER

A. Introduction

An overview of the suggested topology is shown in Figure 1. Her two motor stages are individually controlled in this architecture by modified palpitation range modulation (MPWM). To achieve zero voltage zero current switching (ZVZCS) and provide up to 1.1 kW of power, beats are generated at a switching frequency of 85 kHz in his MPWM mode displays performance data

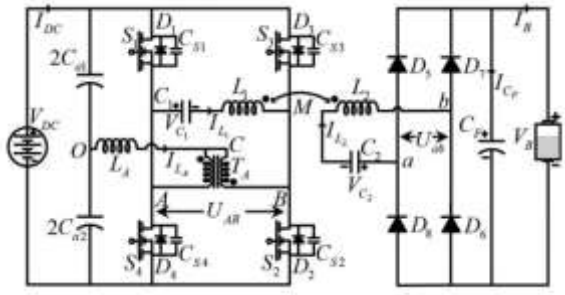

Fig.1 Proposed Converter

Network possibilities for the EV battery tray are suggested in Figure .1. An H ground (traditional) is created by active switches S1–S4 on the primary side and diodes D5–D8 on the secondary side. Along with supporting elements A and TA, Ca1 and Ca2 also function as input implied separators to maintain a soft switching point by BC in the circuit.

Through C1 and C2, the circuit's primary and secondary sides are separately connected to L1 and L2, respectively. MPWM is used to control motor operation. The following theories are taken into account in order to comprehend the proposed engine's operating principle.

1) Internal switching diodes and capacitance, as well as all active and non-resistive biases from motors, DC sources, switches, and capacitors, are excellent.
2) The inductor's electrical series resistance and the motor's winding capacitance are disregarded.
3) The CF and voltage isolation capacitors (Ca = Ca1 = Ca2) are big enough to keep the motor input and output voltage constant.
4) The alluring inductance benefit of TA is disregarded.

B. Operation of Proposed Converter

The steady-state operating principle of the suggested topology is shown to be divided into eight modes (Modes I to VIII), asNetwork possibilities for the EV battery tray are suggested in Figure 3.1. An H ground (traditional) is created by active switches S1–S4 on the primary side and diodes D5–D8 on the secondary side. Along with supporting elements A and TA, Ca1 and Ca2 also function as input implied separators to maintain a soft switching point by BC in the circuit.

Through C1 and C2, the circuit's primary and secondary sides are separately connected to L1 and L2, respectively. MPWM is used to control motor operation. The following theories are taken into account in order to comprehend the proposed engine's operating principle.

5) Internal switching diodes and capacitance, as well as all active and non-resistive biases from motors, DC sources, switches, and capacitors, are excellent.
6) The inductor's electrical series resistance and the motor's winding capacitance are disregarded.
7) The CF and voltage isolation capacitors (Ca = Ca1 = Ca2) are big enough to keep the motor input and output voltage constant.
8) The alluring inductance benefit of TA is disregarded.

C. Operation of Proposed Converter

The steady-state operating principle of the suggested topology is shown to be divided into eight modes (Modes I to VIII), as shown in the picture. The operating waveforms are shown in both Fig. 2 and the figure's operational waveforms.

Fig. 2(a), Mode I (t0 t t1). The lagging current (IL1 ILA) flows from D1 and S2 prior to time t0, and switch S1 turns on with ZVS at this moment. Additionally, there is an implicit distinction between AC and CB because the current ILA starts to rise from ILA(t0).
2) Mode II (t1 t2; Fig. 2(b) and (c) Switch current differential (iS1 iS2) flows from TA(ITA1 ITA2 = ILA) before t0.

Apply KCL to points A and B and use small power savings.

$$iC_{S1} + iC_{S4} = iT_{A2} + iL_1$$

ISSN: 2278-4632
Vol-13, Issue-12, December 2023

$$2iC_{s1} = iL_1 + \frac{iL_1}{2}$$

S2 is still conducting at the beginning of this mode while S1 is off, S3 and S4 were previously off. The switch per acetate capacitor CS1 is being charged by IL1 ILA 2 while the main inductor L1 is decoupled from the DC source. At time t11, VCS1 arrives at VDC. After t11, IL1 creates an ILA change to find a path. This change is rejected by the inductor LA, which discharges CS4 and establishes a current threshold from S2 to S4. When the voltage on CS4 drops to zero, D4 switches on, bringing IS2 to zero (or ZCS for switch S2) as a result.

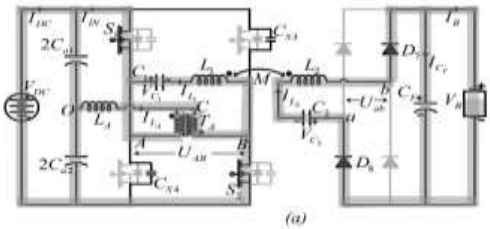
(a)

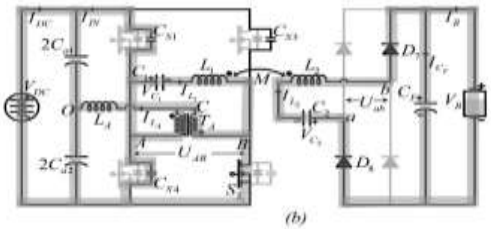
(b)

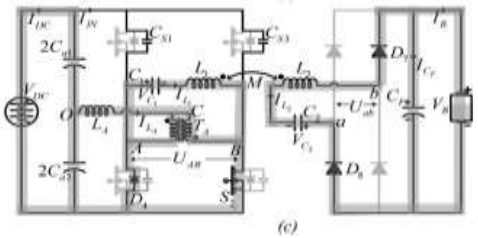
(c)

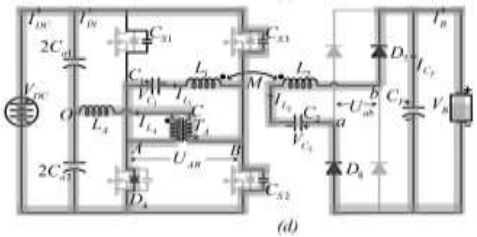
(d)

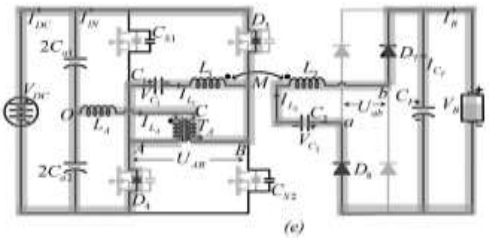
(e)

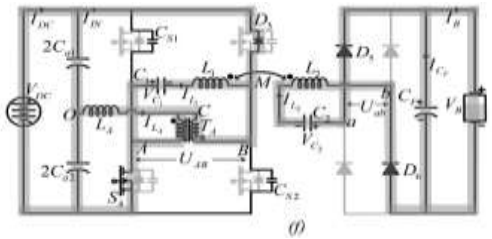
(f)

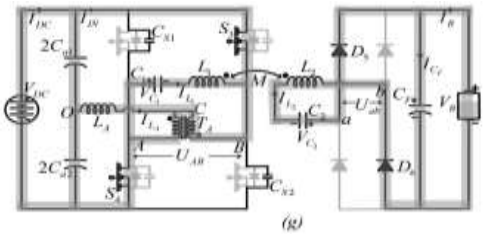
(g)

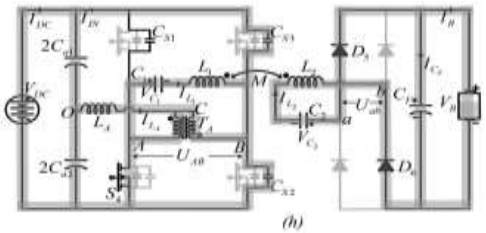
(h)

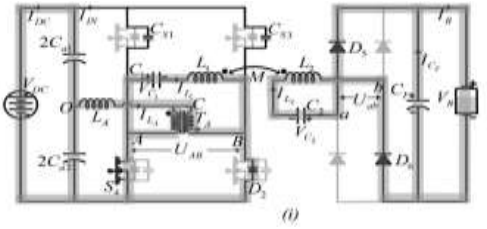
(i)

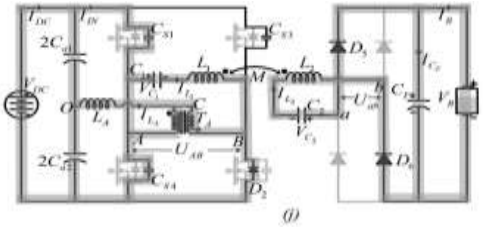
(j)

ISSN: 2278-4632
Vol-13, Issue-12, December 2023

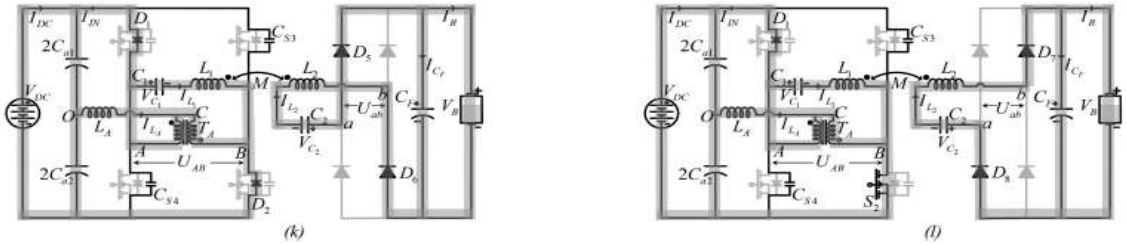

Fig. 2 The suggested battery tray topology's operational modes Mode I (t0, t, and t1) (b) Mode II (First Part) (t1 t t11). Mode II (part 2) (t11 t t2) is in (c).(d) Mode III (first portion) (t2 t tt 21).(e) Mode III (part 2) (t21 t3).Mode IV (t3 t t4).Mode V(t4 t t5) in (g).(h) Mode VI (part-1) (t5 to t51).(i) Mode VI (Part 2) (t51–t6.(j) Mode VII (Part 1) (t6 to t to t61).Mode VII(Part 2)(t61 t t t7) (k).Mode VIII (l) (t7 t t t8).

A) Mode III

(t2 ≤ t Diagram 2(d) and (e) When the other switches are already off, this mode is started by turning off the S2 ZCS. In this phase, the current ILA reaches a positive peak value and subsequently falls towards zero while the per acetic acid capacitor CS2 begins to charge to VDC until t21. Following t21, current IL1 ILA2 flows as a result of the discharge of capacitors CS3 and CS4 and the activation of diodes D2 and D4. The voltage stress at the switch is calculated as follows:

$$v_{S1} = V_{DC} + v_{C1}$$
$$v_{S4} = -v_{C1}$$

B) Mode IV

Fig. 4.2(f), (t3 t t4) Because D4 is turned on and the voltage across S4 is almost zero in this mode of operation, S4 switches on with ZVS. After experiencing a negative peak, the boost inductor current (ILA) rises linearly in the positive direction.

C) Mode V

Fig. 2(g)'s (t4 t t5) S3 is turned on with ZVS in this mode. When IAB's route is complete, it starts to take the shape of a sinusoidal surge, and the voltage between S3 and S4 becomes zero.

D) Mode VI

(Fig. 2(h) and (i), (t5 t t6) By shutting off S3, which causes CS3 to start charging to her VDC att51, this mode is activated. Due to IL1, ILA, the boost inductor current, ILA, rises and then falls, pushes IS4 to enter the ZCS off state.

E) Mode VII

(t6 ≤ t Graph 2(j) and (k) S4 is disabled in this mode at ZCS, and VCS4 ramps up to VDC at att61. ILA starts storming in the positive direction after t61. Current is sent back to the source while diodes D1 and D2 are active.

F) Mode VIII

(t7 ≤ t Fig. 2(l) Switch S2 is activated at ZVS in this mode of operation, switching the current from D2 to S2. The battery voltage and current remain constant in modes I through VIII.

III. SIMULATION RESULTS

Using the top factors as presented, simulations of the suggested topology were carried out in MATLAB/Simulink. Start ZVS for S1 through S4. Table I and Figure 3 A resistance (n) and an inductance (nH) are coupled in series with a DC source in an ideal world. He mimicked the high ground portion of the DC motor by using a MOSFET switch from the Sim Power System library with a resistance of 0 and a capacitance of 870 pF as overvoltage protection. Direct motors, transmitters, and receiver coils are all pulled together by collective inductance. Switches S1–S4 are shown with ZVS ON in Fig. 3.

Gate palpation is used to activate that specific switch when the voltage across it hits zero within the figure Switches S2 and S4's ZCS turn-on is depicted in Figures 5(a) and (b). The current coming from the switch is zero before it reaches the gate palpation target. It may be concluded that the suggested wireless motor maintains ZCZVS as a result. The performance of VC1 is observed in order to calculate the peak value of the compensating capacitor voltage. The input side of the main network is depicted in diagram 4 in the diagram. These findings demonstrate that low input DC-link capacitor values have little impact on motor efficiency. The figure demonstrates it. It can be seen that there is actually less interference in Figures 5(a) and (b). On the other hand, interference in BC voltage

ISSN: 2278-4632
Vol-13, Issue-12, December 2023

and BC current occurs in conventional bowls, which shortens battery life and diminishes bowl effectiveness.

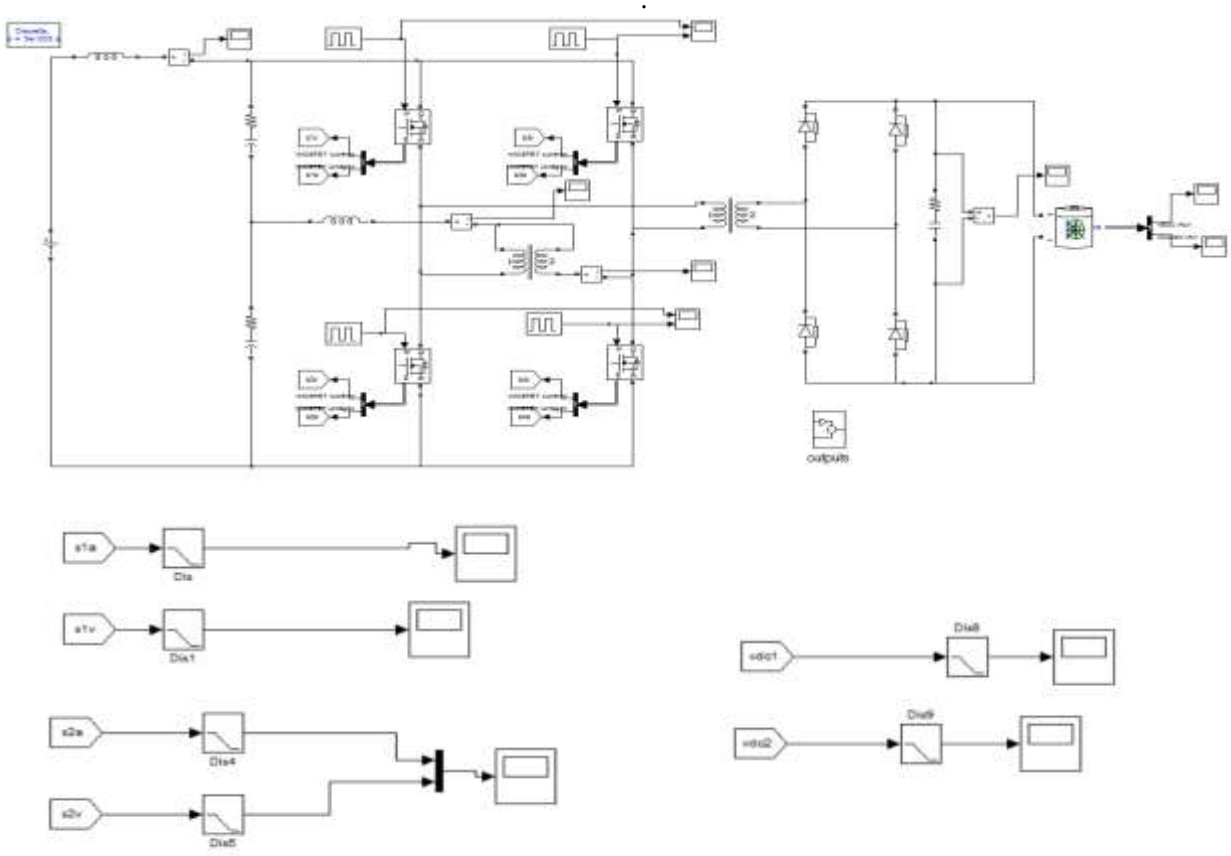

Fig. 3 simulation model

A. Results

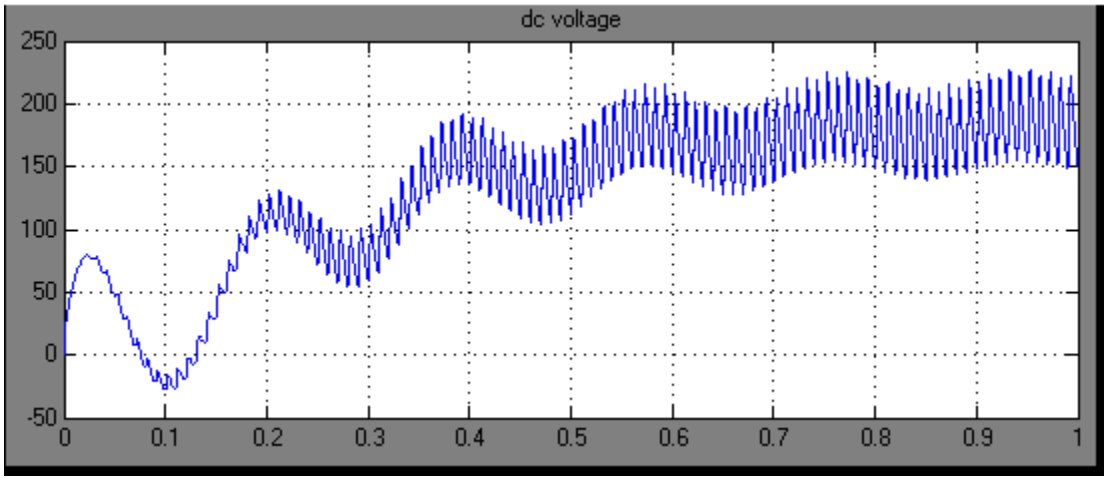

Fig. 4 dc voltage

ISSN: 2278-4632
Vol-13, Issue-12, December 2023

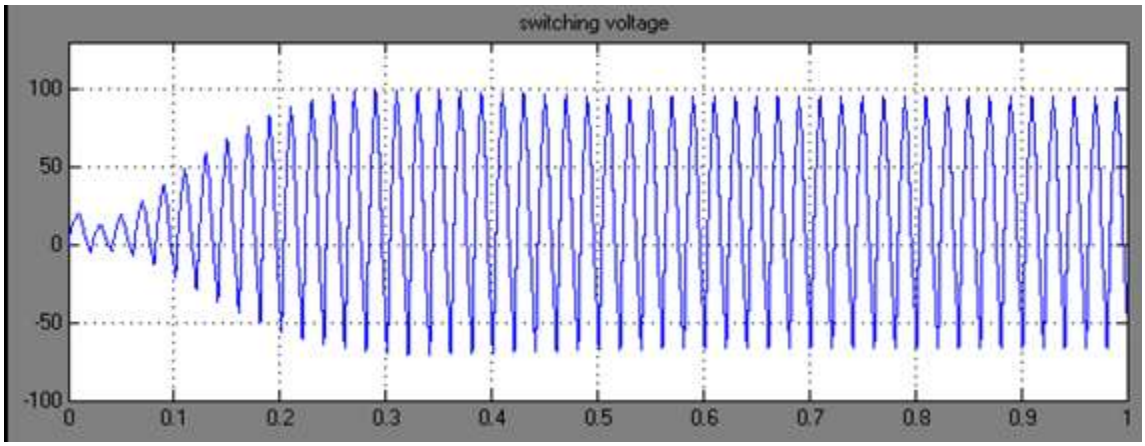

(a)

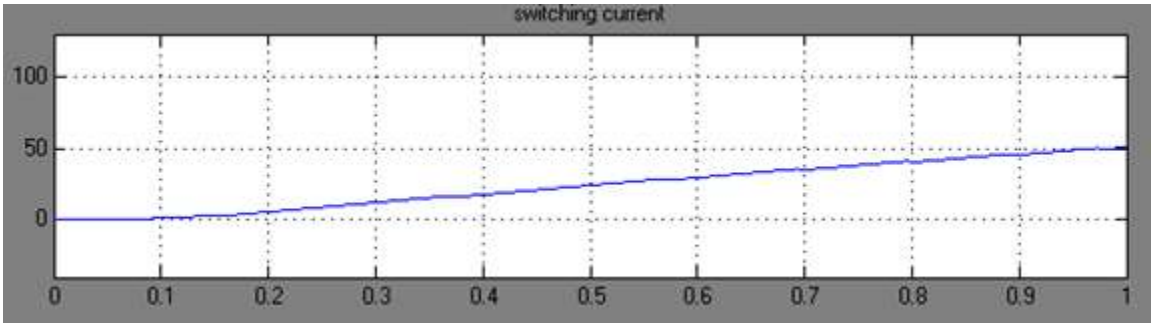

(b)

Fig.5. (a) switching voltage and (b) current

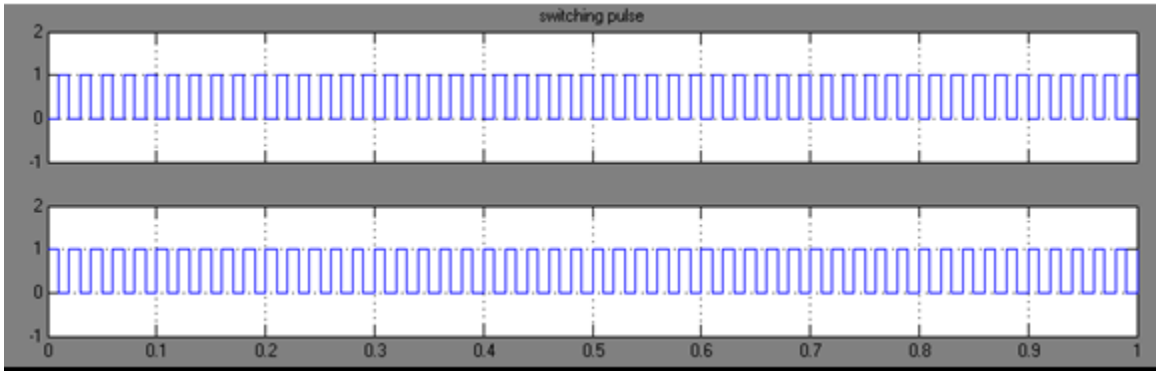

(a)

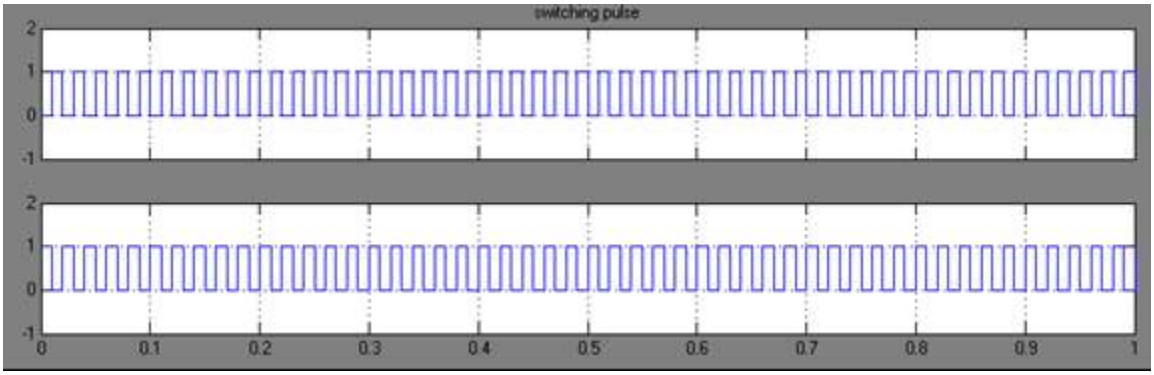

(b)

Fig.6 Gating signals

ISSN: 2278-4632
Vol-13, Issue-12, December 2023

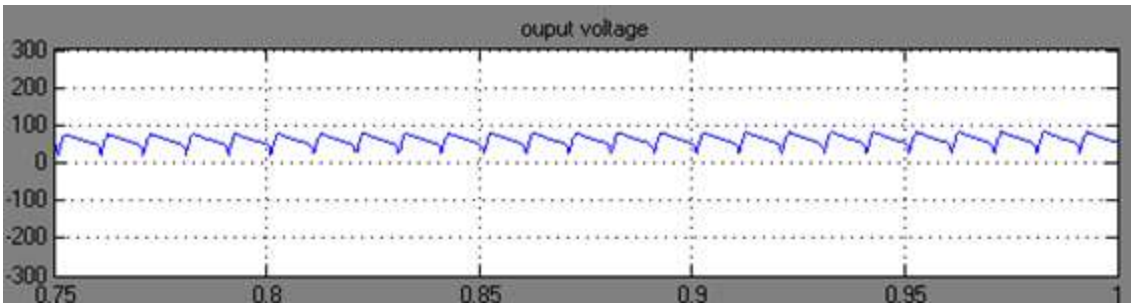

Fig. 7 Output voltage

B. Extension with boost switching

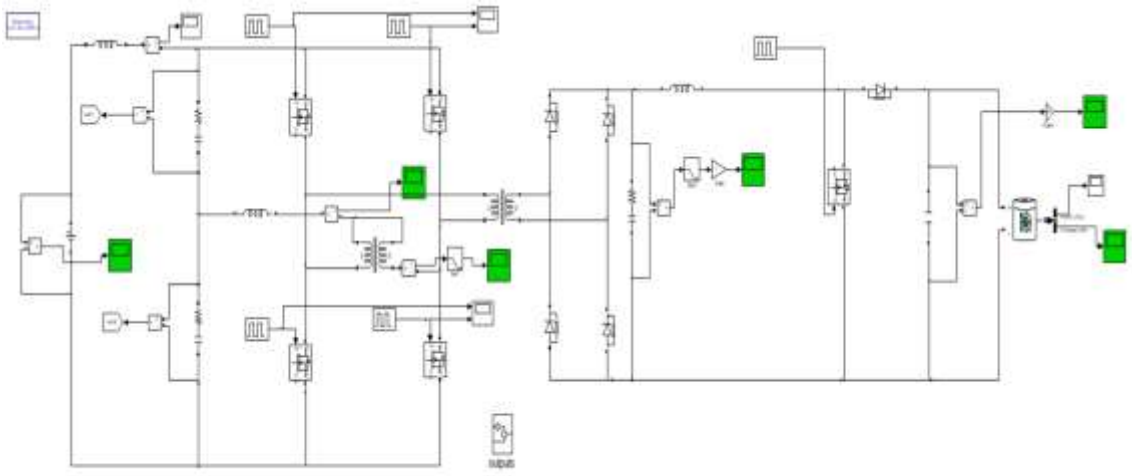

Fig. 8 Simulink model with boost converter

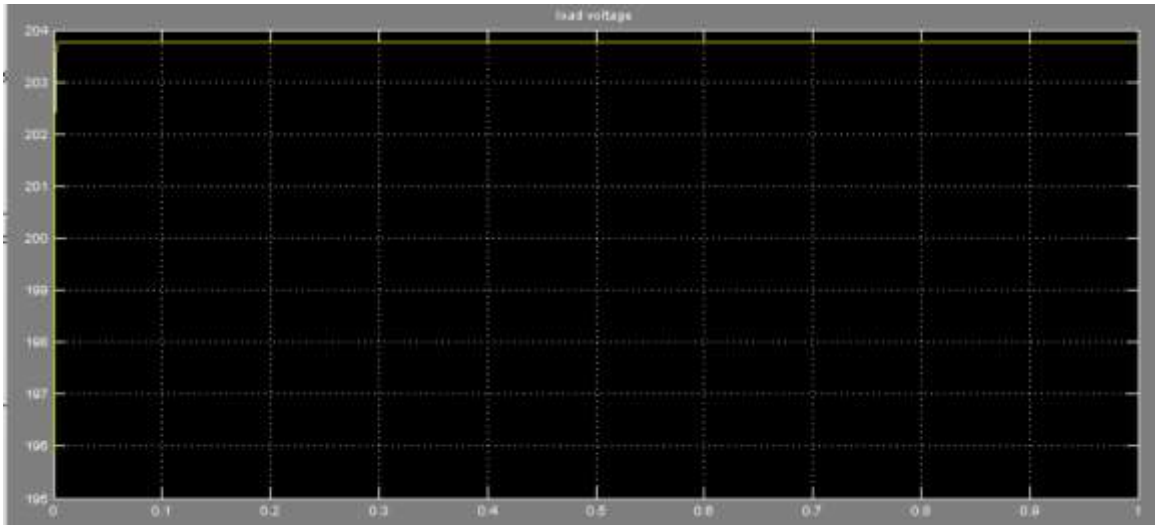

Fig. 9 Output voltage

The Inductive Power Transfer gave better results for electrical vehicle with battery performance.

ISSN: 2278-4632
Vol-13, Issue-12, December 2023

IV. CONCLUSION

For wireless battery trays in electric vehicles, this configuration offered a voltage-fed, series-compensated, grounded ZVZCS topology and associated regulation system. For increased performance over a wide range of input fluctuations, fully grounded DC motors are offered in suitable versions reduces overall expenses by removing the need for high-performance CPUs. He gave theoretical research and modelling to get his ZVZCS with less complicated control. His ZVZCS condition of the suggested topology for the fully charged domain was confirmed by simulation findings. The supplied results reveal low DC-link values and independently lowered capacitance values, as well as low input/relationship voltage and current ripple. The efficiency for combined battery and resistive loads was a good 91.26.

REFERENCES

[1] M. Granowski, I. Dinser and MA. Rosen, ``Comparison of power generation and environment between conventional cold-blooded electric vehicles and hydrogen battery vehicles," J. Stromquellen, vol. 159, no. 2, pp. 1186 – 1193, 2006.

[2] S.B. Peterson, J. Whitacre, and J. Apt: "The Economics of Using Retractable EV Mixer Batteries for Grid Storage," J. Current Sources, vol. 195, no. 8, 2377 – 2384, 2010.

[3] Y. Zhou, M. Wang, H. Hao, L. Johnson and H. Wang, "Requirement Penetration and Driving Force for Plug-in Electric Vehicles - Global Review", "Mitigation Adaptation Strategy Global Change", Vol. 20, no. 5, pp. 777–795, 2015.

[4] B. Nyqvist and M. Nilsson, "Electric vehicle battery pack costs drop temporarily," Nature Climate Change, Vol. 5, No. 2. 4, pp. 329–332, 2015.

[5] W. Chan and C.C. Mi, "Compensation topologies for high-power wireless power transfer systems," IEEE Trans. Veh. Technol., Bd. 65, Nr. 6, S. 4768 – 4778, June 2016.

[6] K. Mude and K. Aditya, "Comprehensive review and analysis of two-element Hall compensation topologies for wireless inductive power transfer systems," Chin.J. handpick.Eng., vol. 5, no. 2, S. 14. – 31. 2019

[7] J. Zhang, L. Wang, Y. Wang, J. Liu, X. Li and G. Ning, "Analysis, design and implementation of precise ZVS angle control for EV battery charging in high-power wireless transmission," IEEE Trans. Ind. Electron., vol. 66, Nr. 5, S. 4075–4085, May 2019.

[8] Y. Jan, L. Wang, Y. Wang, J. Liu, M. Wu, and G. Ning, "Analysis, design, and implementation of a WPT system for charging electric vehicle batteries based on the optimal operating frequency range," IEEE Trans. Power Electron, Bd. 34, Nr. 7, S. 6890 – 6905, July. 2019.

[9] I.E. Tran, V.B. Vu and W. Choi, "Design of High Efficiency Intercoil Wireless Power Transfer System for Electric Vehicle Dish," IEEE Trans. PowerElectron., Vol. 33, no. 1, p. 175-187, January 2018

[10] pp. Moon and G.-W. Moon, "Wireless power transfer system using an asymmetric four-coil resonator for an electric vehicle battery dish," IEEE Trans. Power Electron, Bd. 31, Nr. 10, S. 6844 – 6854, Oktoberfest 2016.

[11] O.C. Onar, M. Chintavari, S.L. Campbell, L.E. Saber and C.P. White, "A Case Study of Vehicle Integration and Interoperability of Wireless Power Transfer Systems," IEEE Trans. Ind.Appl., vol. 55, no. 5, p. 5223 – 5234, September/October 2019.

[12] S. Lee, W. Lee, J. Deng, TD Nguyen and C.C. Water, "A Double-Sided LCC Compensation Network and Its Coordination System for Wireless Power Transfer," IEEE Trans. Veh. Technol., Vol. 64, no. 6, pp. 2261–2273, June. 2015.

[13] C. Liu, S. Ge, Y. Guo, H. Li and G. Cai, "Double-LCL Reverberation Compensation Network for Electric Vehicles, Experimental Study and Analysis of Wireless Power

ISSN: 2278-4632
Vol-13, Issue-12, December 2023

Transfer," IET PowerElectron, vol. 9, Nine. 11, S. 2262–2270, 2016.

[14] C. Xiao, D. Cheng and K. Wei, "Proposal, Trial, and Safety Evaluation of LCC-C Compensated Wireless Charging System for Implantable Cardiac," IEEE Trans. PowerElectron., Vol. 33, no. 6, pp. 4894-4905, June 2018.